Theoretical investigations on the dynamical correlation in double excitations of helium by the *R*-matrix method

Zhen-sheng Yuan,[1,*] Xiao-ying Han,[2] Xiao-jing Liu,[1] Lin-fan Zhu,[1,†] Ke-zun Xu,[1,‡] Lan Voky,[2] and Jia-ming Li[3,2,4,§]
[1]*Hefei National Laboratory for Physical Sciences at Microscale, Department of Modern Physics, University of Science and Technology of China, Hefei 230026, China*
[2]*Center for Atomic and Molecular Nanosciences, Department of Physics, Tsinghua University, Beijing 100084, China*
[3]*Department of Physics, Shanghai Jiao Tong University, Shanghai 200030, China*
[4]*Institute of Physics, Chinese Academy of Sciences, Beijing 100080, China*
(Received 14 May 2004; published 6 December 2004)

The momentum transfer dependence of double excitations of helium were studied theoretically in order to compare with our previous experimental work [Phys. Rev. Lett. **91**, 193203 (2003)]. The calculation was carried out by a series of modified *R*-matrix codes. We elucidate the dynamical correlations in terms of the internal correlation quantum numbers $\mathcal{K}$, $\mathcal{T}$, and A. The generalized oscillator strength densities and Fano profile parameters q, f_a, f, and S of doubly excited states ${}_n(1,0)_2^{+\,1}S^e$, ${}_n(1,0)_2^{+\,1}D^e$, and ${}_n(0,1)_2^{+\,1}P^o$ were reported as functions of the momentum transfer squared K^2. The present theoretical work accompanied by our previous experiment leads to a deep understanding of the optically allowed and optically forbidden double excitations of helium.

DOI: 10.1103/PhysRevA.70.062706 PACS number(s): 34.80.Dp, 31.15.Ar, 32.70.Fw, 32.80.Dz

I. INTRODUCTION

The electron correlation effect plays a fundamental role in atomic and molecular physics. Helium is the simplest system to use to study the electron correlation effect. Since the pioneer experimental work of Madden and Codling [1] and the corresponding theoretical investigations of Fano and coworkers [2,3], the doubly excited states of helium, which were reviewed by Tanner *et al.* [4], have been studied continuously.

The doubly excited states lie above the first ionization threshold. In the early days, evidence of such discrete states was obtained by optical [5] and electron impact [6] experiments. The two Rydberg series of double excitations of helium—i.e., $(sp,2n+)^1P^o$ and $(sp,2n-)^1P^o$—were revealed by Madden and Codling using the photoabsorption method [1]. According to the following theoretical works [7–9], there should be three ${}^1P^o$ series—$(sp,2n+)$, $(sp,2n-)$, and $2pnd$, namely—excited from the ground state ${}^1S^e$ below the $N=2$ threshold of He^+. So the $2pnd$ series was missing in Madden and Codling's measurement [1]. Thereafter, many of experimental studies [10–16] were carried out on the double excitations of helium until the first observation of the missing Rydberg series by Domke *et al.* [17]. With the development of the synchrotron radiation technique, more sophisticated photoionization experiments were performed to acquire the higher Rydberg series above the $N=2$ threshold of He^+ [18–20], decay paths of two-electron excitations [21–25], photoelectron angular distributions [26], threshold energies [27], interseries interferences [28], dipole-quadrupole interference [29], and so on.

Besides the above optical experiments (mostly by the synchrotron radiation method), there were also many of investigations of doubly excited states of helium by the charged-particle impact method. Unlike the optical method, it is possible to observe both optically allowed and optically forbidden transitions to reveal the full richness of the spectrum. Among these studies, most of them were carried out by electron impact [6,30–41] and proton impact [36,42–50], some by other positive ion impacts [32,36,51,52]. Among them, the technique of ejected electron spectroscopy was normally used [31,33–36,38,44,46,49–52]; relatively few experiments used energy loss spectroscopy [30,32,37,39,41,45]. With the proton impact method, there were a few investigations of the angular-dependent behavior of the profile in the ejected electron spectra of doubly excited states [42–48]. For the fast-electron impact and electron-energy loss experiments, as early as in 1963, Silverman and Lassettre observed double excitation $(2s2p)^1P$ and made some discussions of its strength depending on the momentum transfers from 0 to 1.0 a.u. [6]. Later, Wellenstein and collaborators [32] measured the Bethe surface for helium using 25-keV incident electrons with the scattering angles from 0° to 10°. Although the low-energy resolution [2 eV full width at half maximum (FWHM)] precluded them from ruling out contributions from the optically forbidden transitions, they alluded to the possible interest and significance in the momentum-transfer dependence of the Fano parameters. Using 2.5 keV incident energy with a resolution of 0.7 eV FWHM, Fan and Leung [41] measured the generalized oscillator strength density (GOSD) and deconvolved the Fano parameters of the $(1s^2)^1S^e \rightarrow (2s2p)^1P^o$ resonance. Compared with our previous electron impact work by 2.5 keV incident energy and 80 meV FWHM resolution [53], although Fan and Leung's result is not accurate, it was the first attempt to give the

*Electronic address: yuanzs@ustc.edu.cn
†Corresponding author. Electronic address: lfzhu@ustc.edu.cn
‡Electronic address: xukz@ustc.edu.cn
§Electronic address: lijm@sjtu.edu.cn, jmli@cams.tsinghua.edu.cn

momentum-transfer-dependent behavior of the Fano parameters of the $(2s2p)^1P^o$ resonance quantitatively.

Besides the experimental investigations, many of theoretical works were carried out to interpret, predict, and deeply understand the experimental results. The interference between the close channels and open channels around the autoionization region was illustrated theoretically by Fano and Cooper [3], Shore [54], and Mies [55] in the 1960s. In Burke and McVicar's calculation [7] in 1965, resonance states other than the normally known plus-minus series appeared. Sequently, atomic theoreticians developed various methods to deal with doubly excited states of helium, including configuration-interaction (CI) methods [56–60], hyperspherical coordinate methods [9,61–74], close-coupling approximations [7,75,76], *R*-matrix methods [77–84], complex coordinate method [85–90], saddle-point technique [91–95], Feshbach projection formalism [8,96–100], and others [101–106].

In the above methods, most of them presented the resonant energy positions, the resonant widths, and photoabsorption cross sections of these resonances, but a few reported the momentum-transfer-dependent behavior of related parameters in the collision of charged particles with helium, such as the generalized oscillator strength (GOS), whose properties play the central role in the theory of collisions of fast charged particles with atoms and molecules. The GOS with atomic units is written as [107]

$$f(K,E)=\frac{2E}{K^2}\left|\left\langle \psi_f\left|\sum_{j=1}^{n} e^{i\vec{K}\cdot\vec{r}_j}\right|\psi_0\right\rangle\right|^2=\frac{E}{2}\frac{p_0}{p_a}K^2\frac{\mathrm{d}\sigma(K,E)}{\mathrm{d}\Omega}. \tag{1}$$

For the case of fast electron impact, E is the excitation energy, p_0 and p_a are the momenta of the incident electron and scattered electron, respectively, K^2 is the momentum transfer squared, ψ_0 and ψ_f are the N-electron wave functions of the initial (ground) and final states, respectively, and $\vec{r}_j$ is the position vector of the jth atomic electron. The above equation also gives the relationship between the GOS and differential cross section [(DCS), $\mathrm{d}\sigma(K,E)/\mathrm{d}\Omega$].

In Eq. (1), ψ_f is a discrete state. When the discrete state locates above the first ionization threshold, Fano [3] worked out the configuration interaction theory for discrete-continuum interaction. In Fano's theory, the photoabsorption cross section $\sigma(\varepsilon)$ [or the optical oscillator strength density (OOSD)] around the resonance is described by

$$\sigma(\varepsilon)=\sigma_a\frac{(q+\varepsilon)^2}{1+\varepsilon^2}+\sigma_b, \tag{2}$$

where $\varepsilon=(E-E_r)/(\Gamma/2)$ indicates the departure of the incident photon energy E from an idealized resonance energy E_r which pertains to a discrete autoionizing level of the atom with a linewidth Γ. Here σ_a and σ_b represent two portions of the cross section corresponding, respectively, to transitions to states of the continuum that do and do not interact with the discrete autoionizing state. Finally q is a numerical index which characterizes the line profile.

Fano's theory can be applied in the case of nonoptical excitation although only the optical transition operator was considered in Ref. [3]. Following Eq. (2), the GOSD near the resonances is written as

$$\frac{df}{dE}=\sum_i f_{ai}[|q_i\sin\Delta_i-\cos\Delta_i|^2-1]+f_c(E)$$
$$=\sum_i f_{ai}\left(\frac{(q_i+\varepsilon_i)^2}{1+\varepsilon_i^2}-1\right)+f_c(E), \tag{3}$$

where f_{ai} represents the relevant continuums involving interference with the ith resonance, $f_c(E)$ is the total continuum GOSD, which includes both parts that interfere and do not interfere with resonances, Δ_i is the phase parameter due to configuration interaction, $\varepsilon_i=-\cot\Delta_i=(E-E_{ri})/(\Gamma_i/2)$, and q_i have the same meanings as those in Eq. (2), respectively.

In Fano's theory [3], the parameter q_i can be described as

$$q_i=\frac{(\Phi_i|T|\Phi_0)}{\pi V_E^*(\psi_E|T|\Phi_0)}, \tag{4}$$

where Φ_i is the ith "modified" discrete state, ψ_E is the unperturbed continuum state, Φ_0 is the initial state, T is the transition operator, and V_E is the discrete-continuum interaction matrix element. So q_i represents the ratio of transition amplitude to the "modified" discrete state Φ_i and to the unperturbed continuum states ψ_E. For the optical excitation, T is the dipole transition operator $\Sigma_j\vec{r}_j$, while for the present investigation of the GOSD, it is the multipole transition operator $\Sigma_j e^{i\vec{K}\cdot\vec{r}_j}$ instead.

The ratio parameter ρ^2 is defined as

$$\rho_i^2=\left.\frac{f_{ai}(K,E)}{f_c(K,E)}\right|_{E=E_{ri}}. \tag{5}$$

For a specific resonance, the integrated GOS f_i of the "modified" embedded discrete state is expressed as [3]

$$f_i=\int f_{ai}q_i^2\sin^2\Delta_i dE=\frac{\pi\Gamma_i}{2}f_{ai}\,q_i^2|_{E=E_{ri}}, \tag{6}$$

since f_{ai} varies very slowly with E. Note that, for a window-type resonance, f_i always is 0 because $q_i=0$, in spite of degree of the interference between the discrete state and continuum. In order to represent the relevant strength involving interference between the embedded discrete state and the relevant continuum as a whole, an integrated resonance strength S_i was introduced as

$$S_i=f_i+\frac{\pi\Gamma_i}{2}f_{ai}\,q_i^2|_{E=E_{ri}}=\frac{\pi\Gamma_i}{2}(q_i^2+1)f_{ai}\,q_i^2|_{E=E_{ri}}. \tag{7}$$

In our previous work [53], using the fast-electron energy loss spectrometer (EELS), we measured the GOSD's for the doubly excited states of helium below the $N=2$ threshold of He^+ and obtained the parameters q_i and f_{ai} in Eq. (3). Both parameters show a dependence on momentum transfer, which indicates the dynamical electron correlation effect for the two excited electrons. And the parameters ρ_i^2, f_i, and S_i were also calculated according to Eqs. (5)–(7). Theoretically,

in the present work, by introducing the multipole transition elements into the previous *R*-matrix code [80,108–112], the GOSD's in the same energy region were calculated by *R*-matrix theory, and subsequently the corresponding parameters q_i and f_{ai} were deconvolved from the calculated GOSD's. Through a comparison between the experimental and theoretical results, we found that the resonance structures—i.e., q_i parameters—agreed well, but differences still existed for the absolute GOSD's, especially for the case with higher momentum transfer. In the following sections, *R*-matrix theory will be introduced briefly in Sec. II; then, the results and discussions will be presented in Sec. III. Finally some conclusions and outlooks based on the above investigations will be included in Sec. IV.

II. *R*-MATRIX THEORY

One can refer to previous publications [80,108–113] for a detailed description of *R*-matrix theory. Here we just give a brief introduction to *R*-matrix theory and the present implantation of the multipole transition matrix element to the previous codes (also see Ref. [113]).

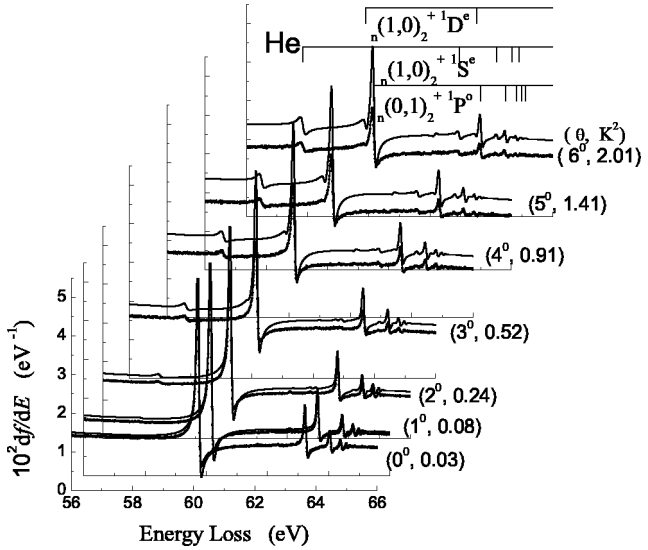

FIG. 1. The measured (points with solid line) [53] and calculated (thin solid line) GOSD's.

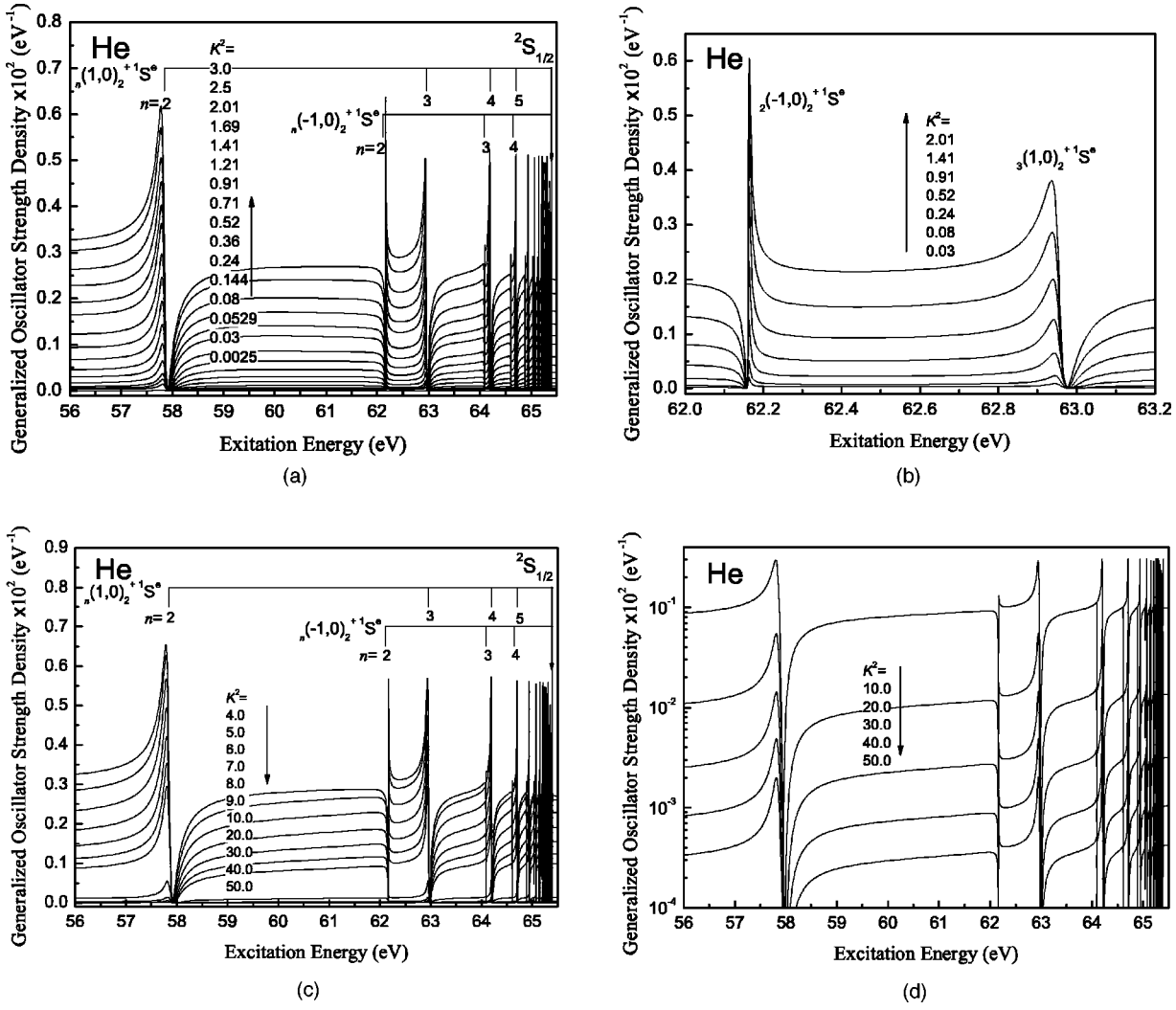

FIG. 2. The GOSD's for the monopole transition series $^1S^e$.

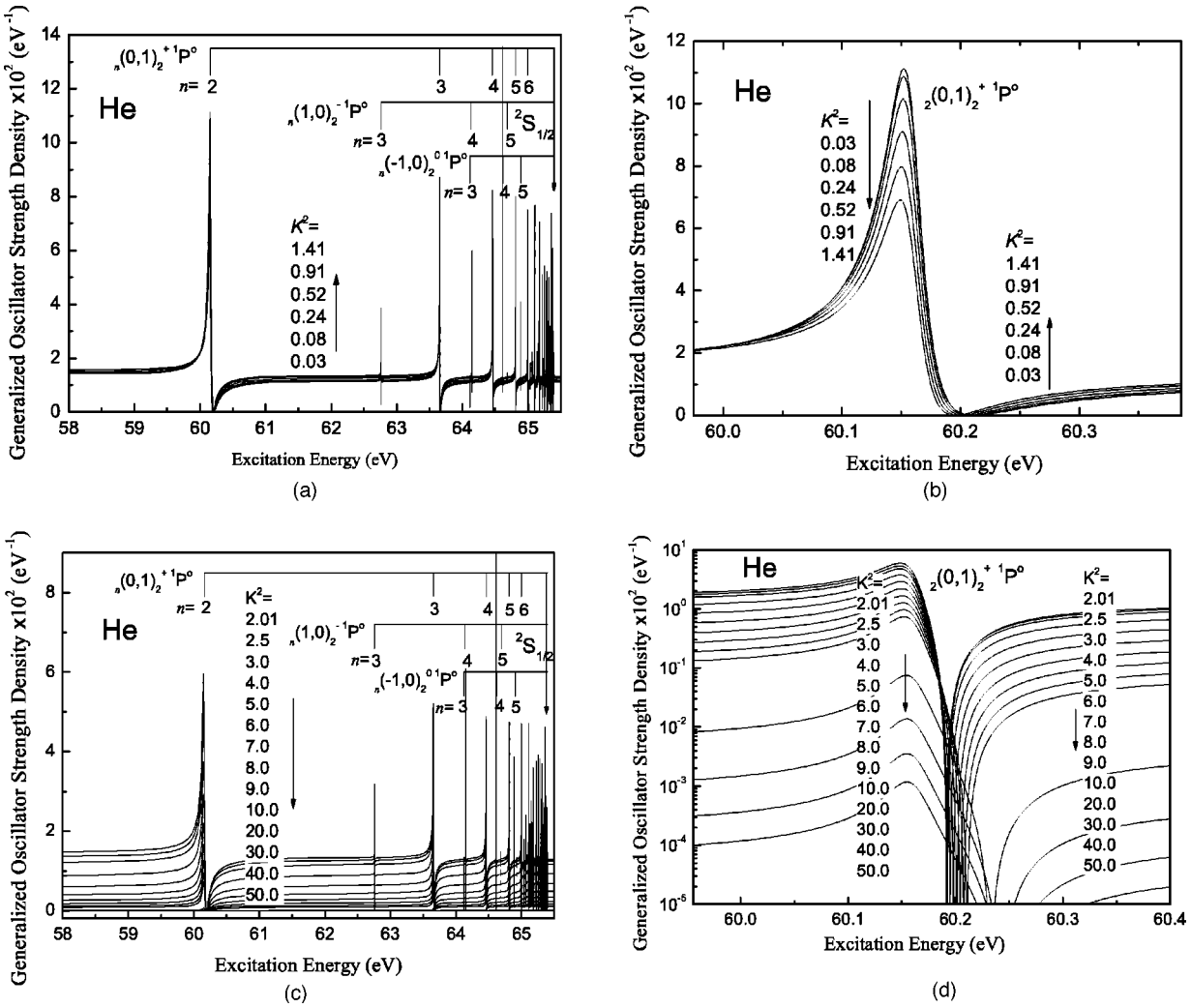

FIG. 3. The GOSD's for the dipole transition series $^1P^o$.

An atomic system can be considered as a scattering system of one electron with an N-electron ionic core:

$$e^- + A_i^+ \rightarrow e^- + A_f^+. \tag{8}$$

The $(N+1)$-electron scattering system is divided into two regions according to the position of the scattered electron—i.e., an internal region and an external region—by a sphere of radius a centered on the target nucleus. In the internal region $r \leqslant a$, where r is the relative coordinate of the scattered electron and the target nucleus, electron exchange and correlation between the scattered electron and the N-electron target are important and the $(N+1)$-electron collision complex behaves in a similar way to a bound state. Consequently a CI expansion of this complex, analogous to that used in bound-state calculations, is adopted. In the external region $r > a$, electron exchange between the scattered electron and the target can be neglected if the radius a is chosen large enough so that the charge distribution of the target is contained within the sphere. The scattered electron then moves in the long-range multipole potential of the target. This potential is local and the solution can be obtained by an asymptotic expansion using perturbation theory. The two regions are linked by the R matrix on the boundary.

In the inner region $r \leqslant a$, the wave function can be written as

$$\Psi = \sum_k A_{Ek} \psi_k, \tag{9}$$

where ψ_k is the energy-independent basis states expanded in the form

$$\psi_k(x_1 \cdots x_{N+1}) = \mathcal{A} \sum_{ij} c_{ijk} \bar{\Phi}_i(x_1 \cdots x_N; \hat{r}_{N+1} \sigma_{N+1}) \frac{1}{r_{N+1}} u_{ij}(r_{N+1}) + \sum_j d_{jk} \chi_j(x_1 \cdots x_{N+1}), \tag{10}$$

where $\mathcal{A}$ is the antisymmetrization operator which accounts for electron exchange between the target electrons and the free electron (with the continuum orbitals u_{ij}) and $\bar{\Phi}_i$ are the channel functions, which are obtained by coupling the target states Φ_i with the angular and spin functions of the scattered electron to form states of the total angular momentum and parity. The quadratically integrable (L^2) functions χ_j, which

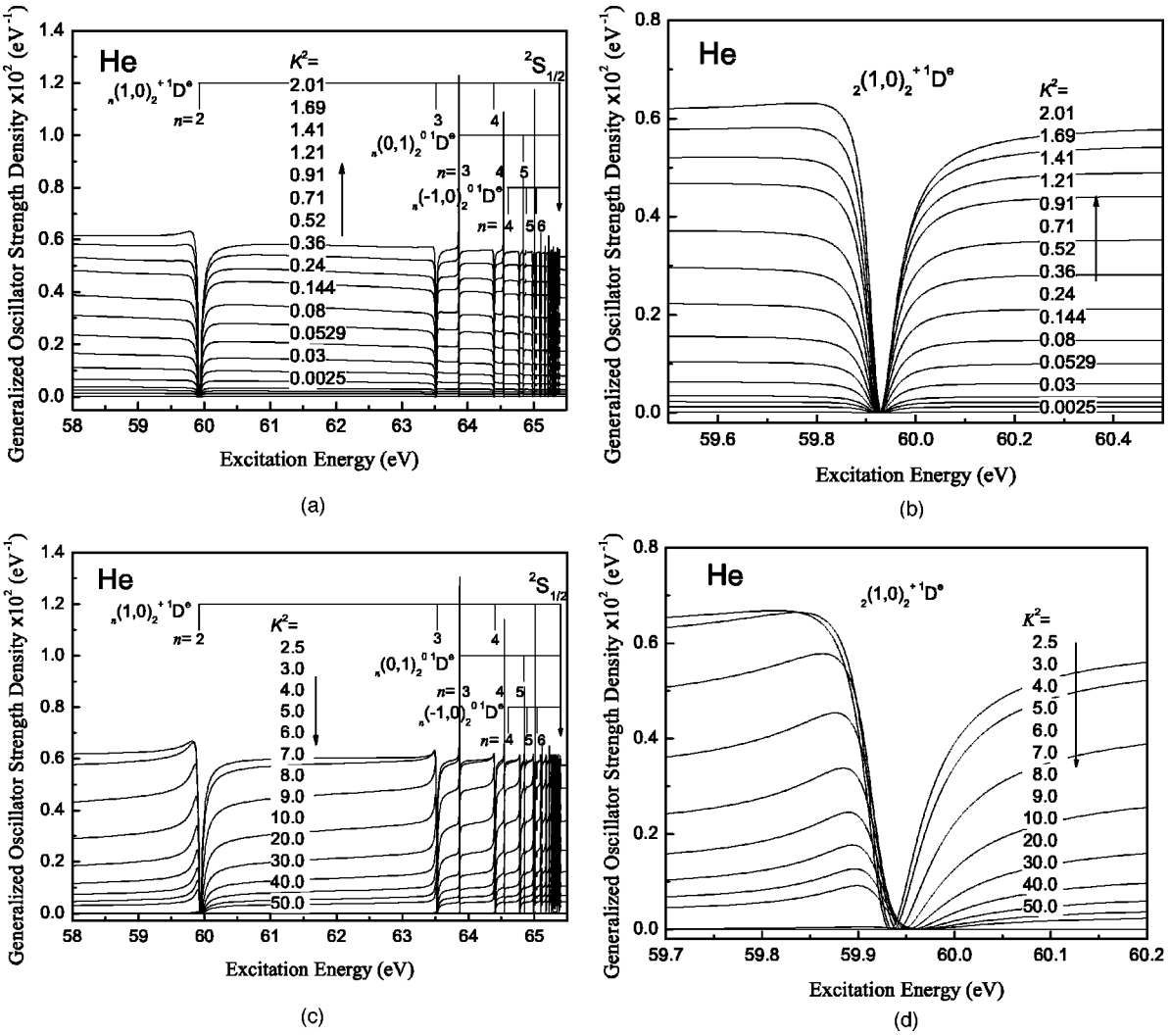

FIG. 4. The GOSD's for the quadrupole transition series $^1D^e$.

vanish at the surface of the internal region, are formed from the bound orbitals and are included to ensure completeness of the total wave function.

In the external region, the colliding electron is outside the atom and can be considered distinct from the N target electrons. The total wave function is expanded in the form

$$\Psi(x_1 \cdots x_{N+1}) = \sum_i \overline{\Phi}_i(x_1 \cdots x_N; \hat{r}_{N+1}\sigma_{N+1}) \frac{1}{r_{N+1}} F_i(r_{N+1}), \tag{11}$$

where $\overline{\Phi}_i$ are the same set of channel functions used in Eq. (10), but now no antisymmetrization is required, and $F_i(r)$ is the wave function of the $(N+1)$th electron.

Using the nonrelativistic R-matrix wave functions, we can write the GOS (or GOSD) in the frame of the first Born approximation [107] as (all variations in atomic unit):

$$f(K,E) = \frac{2E}{K^2}|M_f(K)|^2 = \frac{2E}{K^2}\left|\left\langle \Psi_f \left| \sum_{m=1}^{N+1} e^{i\vec{K}\cdot r_m} \right| \Psi_0 \right\rangle\right|^2. \tag{12}$$

The multipole transition operator can be expressed as

$$e^{i\vec{K}\cdot\vec{r}_m} = \sum_l (2l+1) i^l j_l(Kr_m) P_l(\cos\theta). \tag{13}$$

Considering the summation of the final states (the same energy level with different magnetic quantum numbers) and average of the initial states, the GOS (or GOSD, if the final state is a continuum state) can be written as

$$f(K,E) = \frac{2E}{K^2}\frac{1}{(2L_0+1)(2S_0+1)}|M_f(K)|^2 = \frac{2E}{K^2}\frac{1}{(2L_0+1)(2S_0+1)}$$

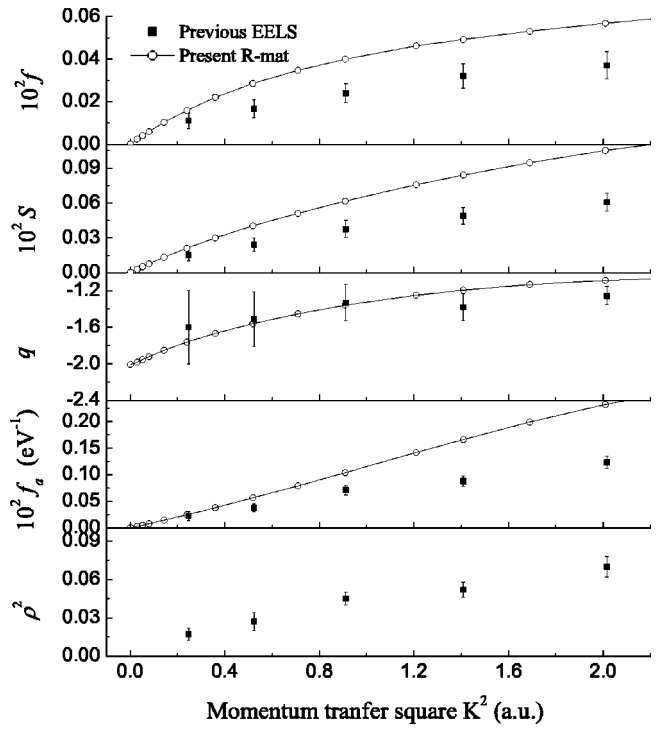

FIG. 5. The fitted Fano parameters f, S, q, f_a, and ρ^2 of ${}_2(1,0)_2^+ {}^1S^e$ of helium as a function of K^2, obtained from the previous EELS [53] and the present theoretical spectra.

$$\times \left| \left\langle \Psi_f \left| \sum_{l=|L_f-L_0|}^{L_f+L_0} (2l+1) i^l j_l(Kr) P_l(\cos\theta) \right| \Psi_0 \right\rangle \right|^2 . \tag{14}$$

In the previous fast-electron (2.5 keV) EELS experiment [53], only the electric monopole, dipole, and quadrupole transitions were observed. Theoretically, the magnetic and higher-order electric transitions can be neglected because of the rapid decrease of the transition magnitudes according to the transition order [114]. So the above three types of electric transitions (i.e., the transitions from the ground state to ${}^1S^e$, ${}^1P^o$, and ${}^1D^e$) were included in the present R-matrix study. As investigated in our previous calculation [80], the target set with polarized orbitals (1s, 2s, 2p, 3s, 3p, 3d, 4$\bar{s}$, 4$\bar{p}$, 4$\bar{d}$) is adopted in the present work. The first ionization threshold 24.58741 eV was obtained from the NIST online database [115].

The calculated GOSD's are shown in Fig. 1. It can be seen that the features observed in the EELS experiment can be reproduced by the R-matrix calculation. The assignments were adopted from the classification in Ref. [9]. In this classification, a doubly excited state ${}^{2S+1}L^{\pi}$ with one inner electron (principal quantum number N) and one outer electron (principal quantum number n) can be represented as ${}_n(\mathcal{K},\mathcal{T})_N^{A\ 2S+1}L^{\pi}$, where $\mathcal{K}$, $\mathcal{T}$, and A are new internal quantum numbers to describe the correlation between the two excited electrons [9]. A numerical deconvolution procedure [116] based on a least-squares fitting was used to obtain each resonance and the relevant parameters f_{ai} and q_i in Eq. (3) for further comparison with the previous experimental result.

III. RESULTS AND DISCUSSIONS

A. Calculated spectra by *R*-matrix theory

The calculated GOSD's of the three transition series—i.e., monopole ${}^1S^e$, dipole ${}^1P^o$, and quadrupole ${}^1D^e$—are shown in Figs. 2–4.

For the ${}^1S^e$ series in Fig. 2, there are evidently two Rydberg series—i.e., ${}_n(1,0)_2^+ {}^1S^e$ and ${}_n(-1,0)_2^+ {}^1S^e$ ($n=2,3,4,\ldots$). The ${}_n(1,0)_2^+ {}^1S^e$ are a series of resonances with constructive interference in the low-energy wing and destructive interference in the high-energy wing, while the ${}_n(-1,0)_2^+ {}^1S^e$ show a reverse character. The resonance in the former series is much wider than that with the same quantum number n in the later series. The GOSD's rise up when K^2 goes from 0.0025 a.u. to 3.0 a.u. while they fall down when K^2 goes from 4.0 a.u. to 50.0 a.u. The resonances and continuum have the same tendency with K^2. It should be noted that both resonances ${}_2(1,0)_2^+ {}^1S^e$ and ${}_2(-1,0)_2^+ {}^1S^e$ rise up when K^2 goes from 0.0025 a.u. to 3.0 a.u. But the strength

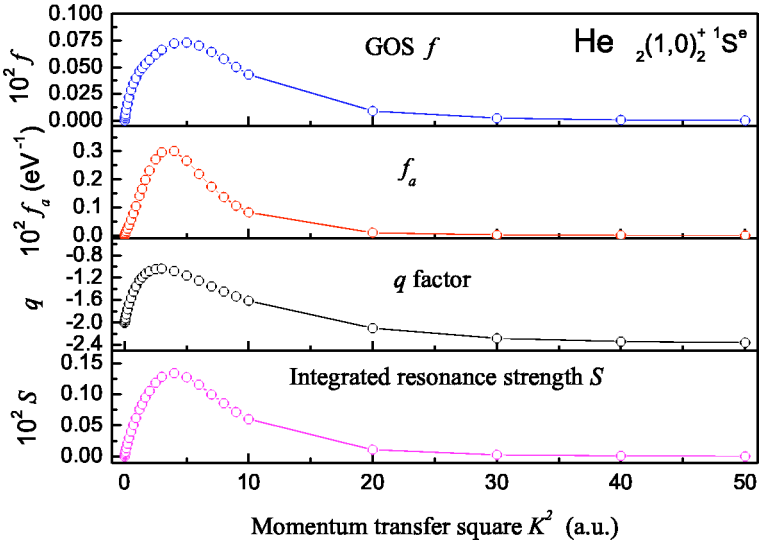

FIG. 6. The fitted Fano parameters f, S, q, and f_a of ${}_2(1,0)_2^+ {}^1S^e$ of helium as a function of K^2 (in the range $K^2=0-50$ a.u.), obtained from the theoretical spectra.

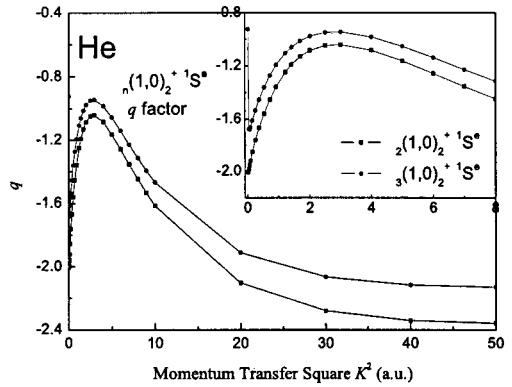

(a)

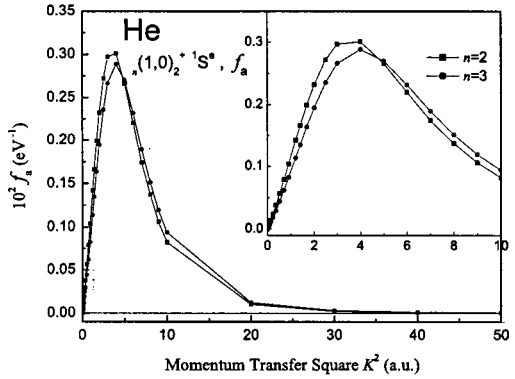

(b)

FIG. 7. The fitted Fano parameters q and f_a of $_n(1,0)_2^+\ ^1S^e$ ($n=2,3$) of helium as a function of K^2 (in the range $K^2=0-50$ a.u.), obtained from the theoretical spectra.

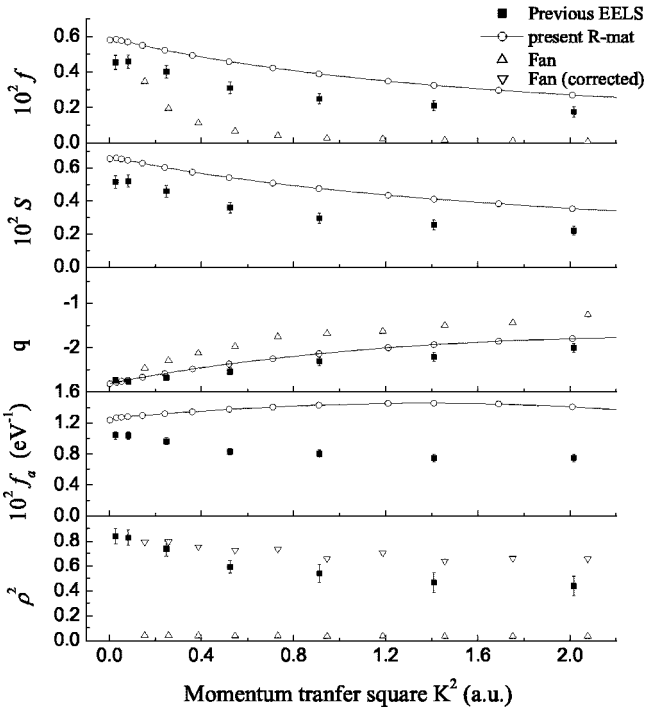

FIG. 8. The fitted Fano parameters f, S, q, f_a, and ρ^2 of $_2(0,1)_2^+\ ^1P^o$ of helium as a function of K^2, obtained from the previous EELS [53] and the present theoretical spectra. The data Fan and Fan (corrected) are taken from [53].

variation of the resonance $_2(-1,0)_2^+\ ^1S^e$ with K^2 is slower than that of $_2(1,0)_2^+\ ^1S^e$, which agrees with the observed spectra [53]. However, at small K^2, the measured strength of the resonance $_2(-1,0)_2^+\ ^1S^e$ is much larger than the calculated result (see Fig. 2 in Ref. [53]). To the best of our knowledge, the dipole-forbidden transition generally has a unremarkable strength relating to the dipole-allowed transition with K^2 as small as 0.03 a.u. (the momentum transfer squared at 0° scattering angle). Therefore, we suspect that for this transition the first Born approximation (FBA) may not be reached. If this suspicion is true, why is it so hard for this transition to reach the FBA?

For the $^1P^o$ series in Fig. 3, there are three Rydberg series—i.e., $_n(0,1)_2^+\ ^1P^o$ ($n=2,3,4,\ldots$), $_n(1,0)_2^-\ ^1P^o$ ($n=3,4,5,\ldots$), and $_n(-1,0)_2^0\ ^1P^o$ ($n=3,4,5,\ldots$). It can be seen that the resonances in the first series are much wider than those in the other two series, which was discussed in Ref. [80]. For the two ultranarrow series, the selection of basis sets and the consideration of long-range potentials result in different resonant structures in R-matrix calculations [80], which is beyond the present discussion. The strength of the resonance $_2(0,1)_2^+\ ^1P^o$ falls down monotonically when K^2 goes from 0.0025 a.u. to 50 a.u., while the strength of the continuum rises up for K^2 from 0.0025 a.u. to 1.41 a.u. and falls down for K^2 from 2.01 a.u. to 50 a.u.

For the $^1D^e$ series in Fig. 4, there are also three Rydberg series—i.e., $_n(1,0)_2^+\ ^1D^e$ ($n=2,3,4,\ldots$), $_n(0,1)_2^0\ ^1D^e$ ($n=3,4,5,\ldots$), and $_n(-1,0)_2^0\ ^1D^e$ ($n=3,4,5,\ldots$). For small K^2, the first series is a "window-type" resonant series, but becomes more asymmetric with an increase of K^2. The GOSD's rise up when K^2 goes from 0.0025 a.u. to 2.01 a.u. and then fall down when K^2 goes from 2.5 a.u. to 50 a.u. This tendency with K^2 is same for the resonances and the continuums.

In Fig. 1, we present the calculated GOSD's accompanied by the experimental results. The original calculated spectra ($^1S^e$, $^1P^o$, and $^1D^e$) were convoluted by a Gaussian instrument function (with 80 meV FWHM) and then summed up to construct the total spectra. The calculated and measured resonant structures agree well with each other and have a similar K^2 dependence on the momentum transfer K^2. The agreement between the measured and calculated absolute values of the GOSD's is good at small scattering angles, but becomes worse with an increase of scattering angle. The differences may come from the fact that the previous incident energy 2.5 keV is not high enough for this excitation energy region (about 60 eV) to reach the FBA, while the present calculation is based on the FBA. It is indeed valuable work to conduct further investigations of these properties from both experimental and theoretical aspects.

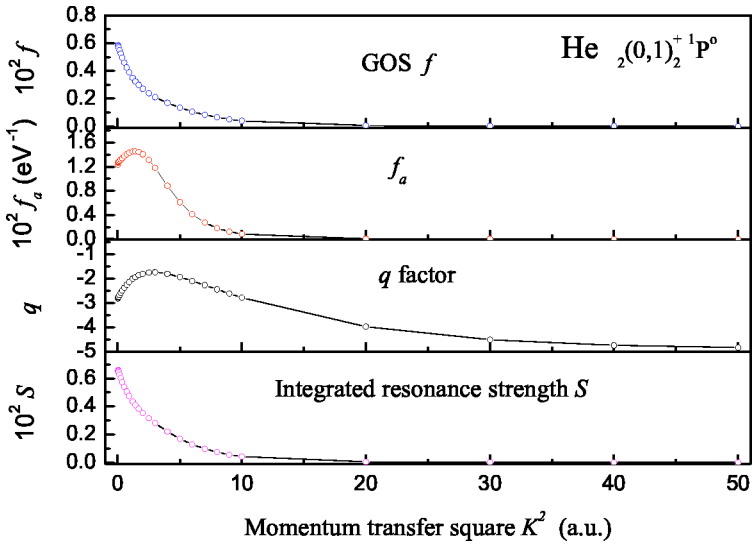

FIG. 9. The fitted Fano parameters f, S, q, and f_a of $_2(0,1)_2^+ {}^1P^o$ of helium as a function of K^2 (in the range $K^2=0-50$ a.u.), obtained from the theoretical spectra.

B. Momentum-transfer-dependent behavior of the Fano parameters

In order to give a quantitative description of the momentum-transfer dependence of the Fano parameters in Eq. (3), each resonance was deconvolved from the GOSD's at each K^2 by a least-squares fitting program [116]. In the following sections, we will discuss these parameters.

1. Electric monopole transition $_n(1,0)_2^+ {}^1S^e$

The fitted Fano parameters of the $_2(1,0)_2^+ {}^1S^e$ resonance are shown in Fig. 5. It can be seen that the theoretical q factors at each K^2 agree with the experimental results within the experimental uncertainties. It is a resonance with constructive interference in the low-energy wing and destructive interference in the high-energy wing since the sign of q is negative for all K^2. The $|q|$ decreases smoothly from 2.0 to 1.2 in the K^2 range $0\rightarrow 2.01$ a.u. It indicates that the transition amplitude into the "modified" discrete state becomes larger with K^2 than that into the relevant continuum. The f, S, and f_a of $_2(1,0)_2^+ {}^1S^e$ increase with K^2 (both experimentally and theoretically), showing the typical behaviors of dipole-forbidden transitions. But for these parameters, the theoretical results vary faster with K^2 than the experimental ones, and the difference between them becomes larger with K^2—e.g., the theoretical f_a at $K^2=2.01$ is 2 times that obtained from the experimental spectrum.

The three parameters—i.e., interfering continuum f_a, integrated GOS f, and resonance strength S—have a similar variation with K^2. Concerning the magnitudes, we can see that f is close to S. This indicates that when $|q|$ is large, f is comparable to S (i.e., $q^2\sim 1+q^2$). So all three parameters can properly describe the momentum-dependent behavior of the resonance $_2(1,0)_2^+ {}^1S^e$.

In Fig. 6, the parameters f, f_a, q, and S of $_2(1,0)_2^+ {}^1S^e$ as a function of K^2 in a wider momentum-transfer range are given. For the four parameters, after a rise below $K^2=5$ a.u., they descend in a long range of $K^2=5\rightarrow 50$ a.u..

The parameters q and f_a of $_n(1,0)_2^+ {}^1S^e$ $(n=2,3)$, which belong to the same Rydberg series, are shown in Fig. 7. We

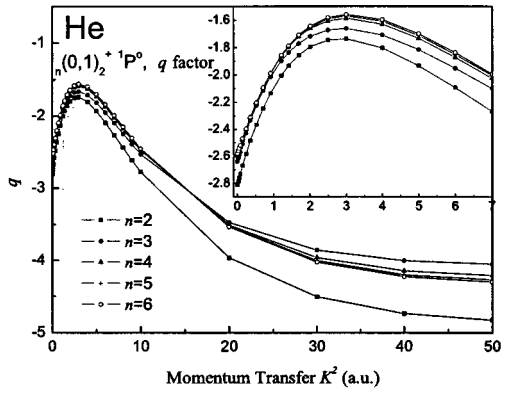

(a)

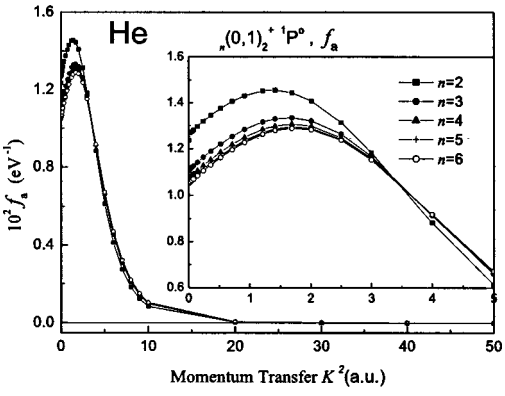

(b)

FIG. 10. The fitted Fano parameters q and f_a of $_{2,3,4,5,6}(0,1)_2^+ {}^1P^o$ of helium as a function of K^2 (in the range $K^2=0-50$ a.u.), obtained from the theoretical spectra.

can see that the two Rydberg states have similar momentum-transfer dependent behavior. It is strange that from $K^2=0.0025$ to 0.03 a.u., the $|q|$ of ${}_3(1,0)_2^+\,{}^1S^e$ jumps up to −0.9 rather than decrease monotonically. We think that this may come from the interferences between the resonances ${}_3(1,0)_2^+\,{}^1S^e$ and ${}_2(-1,0)_2^+\,{}^1S^e$.

2. Electric dipole transition ${}_n(0,1)_2^+\,{}^1P^o$

The fitted Fano parameters of the ${}_2(0,1)_2^+\,{}^1P^o$ resonance are shown in Fig. 8. Also, the theoretical and experimental q factors agree well with each other at each K^2. As K^2 increases, the GOS f and the resonance strength S decrease, showing the typical behaviors of dipole-allowed transitions. The $|q|$ decreases slowly with K^2. It indicates that the transition amplitude into the "modified" discrete state decreases more quickly than that into the relevant continuum. Like the case in the electric monopole transition ${}_2(1,0)_2^+\,{}^1S^e$, the parameters f, f_a, and S obtained from the R-matrix calculation are larger than those obtained from the EELS experiment. Especially for the f_a, the theoretical result rises up below $K^2=1.4$ a.u. and the experimental one descends in the same K^2 region.

In Fig. 9, the parameters f, f_a, q, and S of ${}_2(0,1)_2^+\,{}^1P^o$ as a function of K^2 in a wider momentum-transfer range are given. The parameters f and S descend monotonically in the whole momentum-transfer range, while the parameters f_a and q rise up at low momentum transfer and then descend with K^2. At large K^2, the q parameter reaches −5.

As shown in Fig. 10, for the Rydberg series ${}_n(0,1)_2^+\,{}^1P^o$ ($n=2-6$), the resonance profiles exhibit similar behaviors as the K^2 increases.

3. Electric quadrupole transition ${}_n(1,0)_2^+\,{}^1D^e$

The fitted Fano parameters of the ${}_2(1,0)_2^+\,{}^1D^e$ resonance are displayed in Fig. 11. There are large discrepancies between the theoretical and experimental parameters except for the integrated GOS f although their variation tendencies are similar. Remembering the similar cases in Figs. 5 and 8, we suspect that this may come from the reasons as discussed in Sec. III A: i.e., the experimental incident energy 2.5 keV is not high enough for this excitation energy region (about 60 eV) to reach the FBA. This weak resonance, which overlaps strongly with ${}_2(1,0)_2^+\,{}^1P^o$, may be affected by this strong resonance.

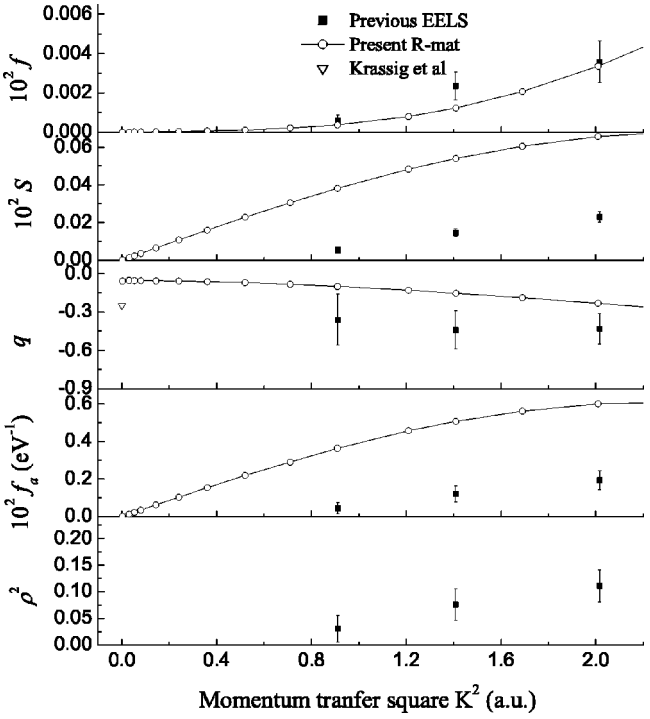

FIG. 11. The fitted Fano parameters f, S, q, f_a, and ρ^2 of ${}_2(1,0)_2^+\,{}^1D^e$ of helium as a function of K^2, previous EELS [53], and the present theoretical spectra.

The agreement between the observed and calculated integrated resonances f is satisfied. However, it should be noted that f depends directly on q and f_a. Then, the cooperation of the two parameters makes this agreement even when discrepancies exist between measured and calculated q and f_a. The magnitude of calculated S is 10 times larger than that of calculated f and is more appropriate to describe the strength of the resonance.

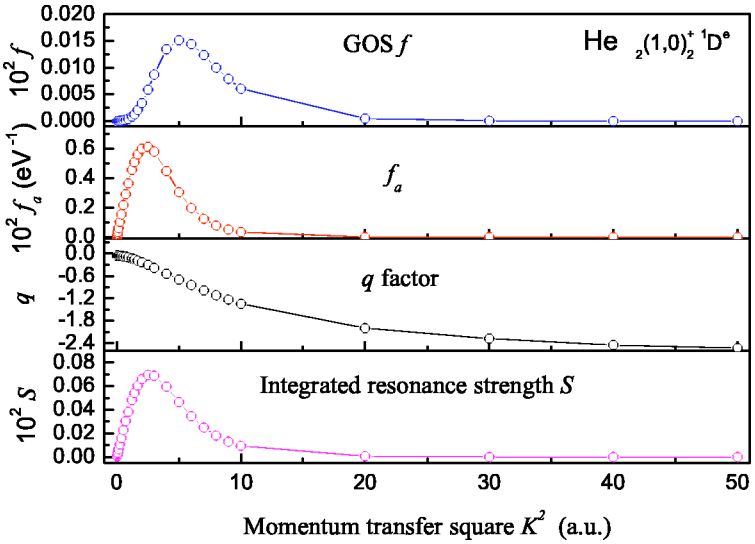

FIG. 12. The fitted Fano parameters f, S, q, and f_a of ${}_2(1,0)_2^+\,{}^1D^e$ of helium as a function of K^2 (in the range $K^2=0-50$ a.u.), obtained from the theoretical spectra.

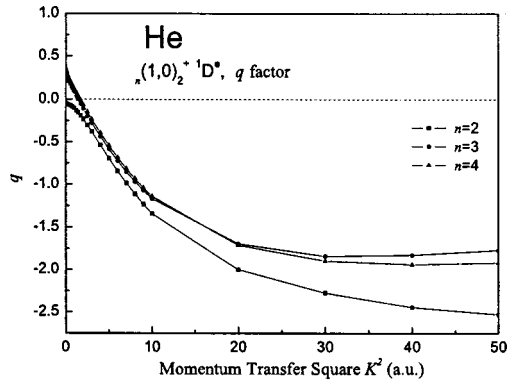

(a)

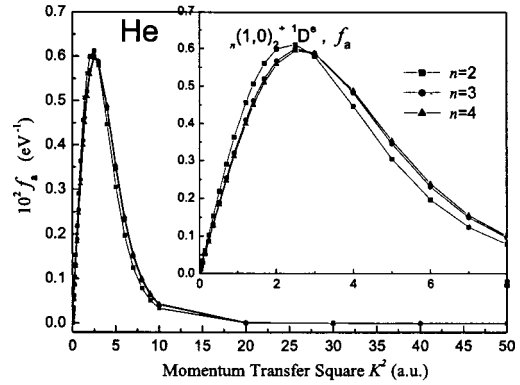

(b)

FIG. 13. The fitted Fano parameters q and f_a of $_{2,3,4}(1,0)_2^{+}\,{}^1D^e$ of helium as a function of K^2 (in the range $K^2=0-50$ a.u.), obtained from the theoretical spectra.

The present theoretical $|q|$ is less than the observed result. The f, S, f_a, and ρ^2 of $_2(1,0)_2^{+}\,{}^1D^e$ increase with K^2, showing the typical behaviors of quadrupole transitions.

In Fig. 12, the parameters f, f_a, q, and S of $_2(1,0)_2^{+}\,{}^1S^e$ as a function of K^2 in a wider momentum-transfer range are given. The parameters f_a and S have a maximum at $K^2 \sim 2.5$ a.u., and f has a maximum at $K^2 \sim 5$ a.u. The q factor descends in the whole momentum transfer range.

The parameters q and f_a of $_n(1,0)_2^{+}\,{}^1D^e$ ($n=2,3,4$), are shown in Fig. 13. We can see that the three Rydberg states have the similar momentum-transfer-dependent behavior. It is interesting that the q factors of resonance $_n(1,0)_2^{+}\,{}^1D^e$ ($n=3,4$) go from positive, across zero, to negative. This indicates that the resonance profiles transform from destructive interference in the low-energy wing and constructive interference in the high-energy wing to constructive interference in the low-energy wing and destructive interference in the high-energy wing.

IV. CONCLUSIONS

From the above R-matrix study, we obtained the GOS's and Fano profile parameters q, f_a, ρ^2, f, and S of the doubly excited states $_n(1,0)_2^{+}\,{}^1S^e$, $_n(1,0)_2^{+}\,{}^1D^e$, and $_n(0,1)_2^{+}\,{}^1P^o$ as functions of the momentum transfer squared, K^2. It is an advancement in the investigation of helium double excitations. Through these parameters, the dynamical correlations between the two highly excited electrons can be elucidated. The present calculated q factors agree well with the observed result [53] at each K^2, but discrepancies still exist for the parameters f_a, f, and S between the calculated and observed results although they have similar variation tendencies with K^2. We suspect that the previous incident energy 2.5 keV may be not high enough to reach the FBA in this excitation energy region. This is an open question for further experimental and theoretical investigations.

ACKNOWLEDGMENTS

We thank Jun Yan, Yi-zhi Qu, and Zhi-ping Zhong for helpful discussions. Support by the National Nature Science Fund of China (Grant Nos. 10134010 and 10176013), the Youth Foundation of the University of Science and Technology of China, and the National High-Tech ICF Committee in China is gratefully acknowledged.

[1] R. P. Madden and K. Codling, Phys. Rev. Lett. **10**, 516 (1963).
[2] J. W. Cooper, U. Fano, and F. Prats, Phys. Rev. Lett. **10**, 518 (1963).
[3] U. Fano, Phys. Rev. **124**, 1866 (1961); U. Fano and J. W. Cooper, Phys. Rev. **137**, A1364 (1965).
[4] G. Tanner, K. Richter, and J. M. Rost, Rev. Mod. Phys. **72**, 497 (2000).
[5] R. Whiddington and H. Priestley, Proc. R. Soc. London, Ser. A **145**, 462 (1934); H. Priestley and R. Whiddington, Proc. Leeds Philos. Lit. Soc., Sci. Sect. **3**, 81 (1940).
[6] S. M. Silverman and E. N. Lassettre J. Chem. Phys. **40**, 1265 (1963).
[7] P. G. Burke and D. D. McVicar, Proc. Phys. Soc. London **86**, 989 (1965).
[8] K. T. Chung and I. H. Chen, Phys. Rev. Lett. **28**, 783 (1972).
[9] C. D. Lin, Phys. Rev. A **29**, 1019 (1984); Z. Chen and C. D. Lin, *ibid.* **40**, 6712 (1989).
[10] P. R. Woodruff and J. A. R. Samson, Phys. Rev. A **25**, 848 (1982).
[11] H. D. Morgan and D. L. Ederer, Phys. Rev. A **29**, 1901 (1984).
[12] D. W. Lindle, T. A. Ferrett, P. A. Heimann, and D. A. Shirley, Phys. Rev. A **36**, 2112 (1987).
[13] H. Kossmann, B. Krässig, and V. Schmidt, J. Phys. B **21**, 1489 (1988).
[14] M. Zubek, G. C. King, P. M. Rutter, and F. H. Read, J. Phys. B **22**, 3411 (1989).
[15] M. Zubek, G. Dawber, R. I. Hall, L. Avaldi, K. Ellis, and G. C. King, J. Phys. B **24**, L337 (1991).

[16] M. Domke, C. Xue, A. Puschmann, T. Mandel, E. Hudson, D. A. Shirley, G. Kaindl, C. H. Greene, H. R. Sadeghpour, and H. Petersen, Phys. Rev. Lett. **66**, 1306 (1991).
[17] M. Domke, G. Remmers, and G. Kaindl, Phys. Rev. Lett. **69**, 1171 (1992).
[18] M. Domke, K. Schulz, G. Remmers, A. Gutiérrez, G. Kaindl, and D. Wintgen, Phys. Rev. A **51**, R4309 (1995).
[19] K. Schulz, G. Kaindl, M. Domke, J. D. Bozek, P. A. Heimann, A. S. Schlachter, and J. M. Rost, Phys. Rev. Lett. **77**, 3086 (1996).
[20] M. Domke, K. Schulz, G. Remmers, G. Kaindl, and D. Wintgen, Phys. Rev. A **53**, 1424 (1996).
[21] A. Menzel, S. P. Frigo, S. B. Whitfield, C. D. Caldwell, M. O. Krause, J. Z. Tang, and I. Shimamura, Phys. Rev. Lett. **75**, 1479 (1995).
[22] E. Sokell, A. A. Wills, J. Comer, and P. Hammond, J. Phys. B **29**, L83 (1996).
[23] E. Sokell, A. A. Wills, P. Hammond, M. A. MacDonald, and M. K. Odling-Smee, J. Phys. B **29**, L863 (1996).
[24] J.-E. Rubensson, C. Sâthe, S. Cramm, B. Kessler, S. Stranges, R. Richter, M. Alagia, and M. Coreno, Phys. Rev. Lett. **83**, 947 (1999).
[25] M. K. Odling-Smee, E. Sokell, P. Hammond, and M. A. MacDonald, Phys. Rev. Lett. **84**, 2598 (2000).
[26] A. Menzel, S. P. Frigo, S. B. Whitfield, C. D. Caldwell, and M. O. Krause, Phys. Rev. A **54**, 2080 (1996).
[27] D. B. Thompson, P. Bolognesi, M. Coreno, R. Camilloni, L. Avaldi, K. C. Prince, M. de Simone, J. Karvonen, and G. C. King, J. Phys. B **31**, 2225 (1998).
[28] R. Püttner, M. Domke, B. Grémaud, M. Martins, A. S. Schlachter, and G. Kaindl, J. Electron Spectrosc. Relat. Phenom. **101–103**, 27 (1999).
[29] B. Krässig, E. P. Kanter, S. H. Southworth, R. Guillemin, O. Hemmers, D. W. Lindle, R. Wehlitz, and N. L. S. Martin, Phys. Rev. Lett. **88**, 203002 (2002).
[30] J. A. Simpson, G. E. Chamberlain, and S. R. Mielczarek, Phys. Rev. **139**, A1039 (1965).
[31] N. Oda, F. Nishimura, and S. Tahira, Phys. Rev. Lett. **24**, 42 (1970).
[32] H. F. Wellenstein, R. A. Bonham, and R. C. Ulsh, Phys. Rev. A **8**, 304 (1973).
[33] P. J. Hicks and J. Comer, J. Phys. B **8**, 1866 (1975); J. P. van den Brink, G. Nienhuis, J. van Eck, and H. G. M. Heideman, J. Phys. B **22**, 3501 (1989).
[34] G. Gelebart, R. J. Tweed, and J. Peresse, J. Phys. B **9**, 1739 (1976).
[35] N. Oda, S. Tahira, F. Nishimura, and F. Koike, Phys. Rev. A **15**, 574 (1977).
[36] J. O. P. Pedersen and P. Hvelplund, Phys. Rev. Lett. **62**, 2373 (1989).
[37] W. F. Chan, G. Cooper, and C. E. Brion, Phys. Rev. A **44**, 186 (1991).
[38] D. G. McDonald and A. Crowe, J. Phys. B **25**, 4313 (1992).
[39] S. J. Brotton, S. Cvejanovic, F. J. Currell, N. J. Bowring, and F. H. Read, Phys. Rev. A **55**, 318 (1997).
[40] M. J. Brunger, O. Samardzic, A. S. Kheifets, and E. Weigold, J. Phys. B **30**, 3267 (1997).
[41] X. W. Fan and K. T. Leung, J. Phys. B **34**, 811 (2001).
[42] N. Stolterfoht, D. Ridder, and P. Ziem, Phys. Lett. **42A**, 240 (1972).
[43] A. Bordenave-Montesquieu, P. Benoit-Cattin, M. Rodiere, A. Gleizes, and H. Merchez, J. Phys. B **6**, 1997 (1973).
[44] A. Bordenave-Montesquieu, A. Gleizes, P. Moreeto-Capelle, S. Andriamonje, P. Benoit-Cattin, F. Martin, and A. Salin, J. Phys. B **25**, L367 (1992).
[45] W. T. Htwe, T. Vajnai, M. Barnhart, A. D. Gaus, and M. Schulz, Phys. Rev. Lett. **73**, 1348 (1994).
[46] A. Bordenave-Montesquieu, P. Moreeto-Capelle, A. Gleizes, S. Andriamonje, F. Martin, and A. Salin, J. Phys. B **28**, 653 (1995).
[47] M. Schulz, W. T. Htwe, A. D. Gaus, J. L. Peacher, and T. Vajnai, Phys. Rev. A **51**, 2140 (1995).
[48] M. Schulz, Int. J. Mod. Phys. B **9**, 3269 (1995).
[49] A. L. Godunov, V. A. Schipakov, P. Moretto-Capelle, D. Bordenave-Montesquieu, M. Benhenni, and A. Bordenave-Montesquieu, J. Phys. B **30**, 5451 (1997).
[50] P. Moretto-Capelle, D. Bordenave-Montesquieu, A. Bordenave-Montesquieu, A. L. Godunov, and V. A. Schipakov, Phys. Rev. Lett. **79**, 5230 (1997).
[51] M. E. Rudd, Phys. Rev. Lett. **15**, 580 (1965).
[52] D. Burch, J. Bolger, and C. Fred Moore, Phys. Rev. Lett. **34**, 1067 (1975).
[53] X. J. Liu, L. F. Zhu, Z. S. Yuan, W. B. Li, H. D. Cheng, Y. P. Huang, Z. P. Zhong, K. Z. Xu, and J. M. Li, Phys. Rev. Lett. **91**, 193203 (2003).
[54] B. W. Shore, Rev. Mod. Phys. **39**, 439 (1967); Phys. Rev. **171**, 43 (1968).
[55] F. H. Mies, Phys. Rev. **175**, 164 (1968).
[56] D. R. Herrick and O. Sinanoğlu, Phys. Rev. A **11**, 97 (1975).
[57] R. Moccia and P. Spizzo, J. Phys. B **20**, 1423 (1987).
[58] C. Froese Fischer and M. Idrees, J. Phys. B **23**, 679 (1990).
[59] T. N. Chang, Phys. Rev. A **47**, 3441 (1993).
[60] M. Venuti, P. Decleva, and A. Lisini, J. Phys. B **29**, 5315 (1996).
[61] J. Macek, J. Phys. B **1**, 831 (1968).
[62] C. D. Lin, Phys. Rev. A **10**, 1986 (1974).
[63] C. D. Lin, Phys. Rev. A **25**, 76 (1982); **26**, 2305 (1982); **27**, 22 (1983); C. D. Lin and J. H. Macek, *ibid.* **29**, 2317 (1984).
[64] C. D. Lin, Phys. Rev. A **25**, 1535 (1982).
[65] C. D. Lin, Phys. Rev. Lett. **51**, 1348 (1983).
[66] S. Watanabe and C. D. Lin, Phys. Rev. A **34**, 823 (1986).
[67] H. R. Sadeghpour, Phys. Rev. A **43**, 5821 (1991).
[68] J. M. Rost, R. Gersbacker, K. Richter, J. S. Briggs, and D. Wintgen, J. Phys. B **24**, 2455 (1991).
[69] J. M. Rost, S. M. Sung, D. R. Herschbach, and J. S. Briggs, Phys. Rev. A **46**, 2410 (1992).
[70] L. J. Zhang and A. R. P. Rau, Phys. Rev. A **46**, 6933 (1992).
[71] J. Z. Tang, S. Watanabe, and M. Matsuzawa, Phys. Rev. A **48**, 841 (1993); **46**, 2437 (1992).
[72] J. Z. Tang and I. Shimamura, Phys. Rev. A **50**, 1321 (1994).
[73] C. D. Lin, Phys. Rep. **257**, 1 (1995).
[74] T. Morishita, K. I. Hino, S. Watanabe, and M. Matsuzawa, Phys. Rev. A **53**, 2345 (1996).
[75] D. H. Oza, Phys. Rev. A **33**, 824 (1986).
[76] S. Salomonson, S. L. Carter, and H. P. Kelly, Phys. Rev. A **39**, 5111 (1989).
[77] K. A. Berrington, P. G. Burke, W. C. Fon, and K. T. Taylor, J. Phys. B **15**, L603 (1982).
[78] J. A. Fernley, K. T. Taylor, and M. J. Seaton, J. Phys. B **20**, 6457 (1987).

[79] P. Hamacher and J. Hinze, J. Phys. B **22**, 3397 (1989).
[80] J. Yan, Y. Z. Qu, L. Voky, and J. M. Li, Phys. Rev. A **57**, 997 (1998).
[81] T. W. Gorczyca, J.-E. Rubensson, C. Såthe, M. Ström, M. Agâker, D. Ding, S. Stranges, R. Richter, and M. Alagia, Phys. Rev. Lett. **85**, 1202 (2000).
[82] Y. H. Jiang, J. Yan, J. M. Li, J. F. Sun, and L. D. Wan, Phys. Rev. A **61**, 032721 (2000).
[83] H. W. van der Hart and C. H. Greene, Phys. Rev. A **66**, 022710 (2002).
[84] T. Schneider, C. N. Liu, and J. M. Rost, Phys. Rev. A **65**, 042715 (2002).
[85] Y. K. Ho, Phys. Rev. A **23**, 2137 (1981).
[86] Y. K. Ho, Phys. Rev. A **34**, 4402 (1986).
[87] P. Froelich and A. Flores-Riveros, J. Chem. Phys. **86**, 2674 (1987).
[88] P. Froelich and S. A. Alexander, Phys. Rev. A **42**, 2550 (1990).
[89] Y. K. Ho, Phys. Rev. A **48**, 3598 (1993).
[90] A. Bürgers, D. Wintgen, and J.-M. Rost, J. Phys. B **28**, 3163 (1995).
[91] L. J. Wu and J. H. Xi, J. Phys. B **23**, 727 (1990).
[92] J. M. Rost and J. S. Briggs, J. Phys. B **24**, 4293 (1991).
[93] M. K. Chen, Phys. Rev. A **56**, 4537 (1997).
[94] M. K. Chen, Phys. Rev. A **60**, 2565 (1999).
[95] C. N. Liu, M. K. Chen, and C. D. Lin, Phys. Rev. A **64**, 010501(R) (2001).
[96] K. T. Chung and I. H. Chen, Phys. Rev. A **10**, 997 (1974).
[97] A. K. Bhatia and A. Temkin, Phys. Rev. A **11**, 2018 (1975).
[98] A. K. Bhatia and A. Temkin, Phys. Rev. A **29**, 1895 (1984).
[99] A. Macias, F. Martin, A. Riera, and M. Yanez, Phys. Rev. A **36**, 4187 (1987).
[100] J. M. Seminario and F. C. Sanders, Phys. Rev. A **42**, 2562 (1990).
[101] D. R. Herrick and M. E. Kellman, Phys. Rev. A **21**, 418 (1980); D. R. Herrick, M. E. Kellman, and R. D. Poliak, *ibid.* **22**, 1517 (1980).
[102] G. S. Ezra, K. Richter, G. Tanner, and D. Wintgen, J. Phys. B **24**, L413 (1991).
[103] D. Wintgen and D. Delande, J. Phys. B **26**, L399 (1993).
[104] I. Sánchez and F. Martín, Phys. Rev. A **48**, 1243 (1993).
[105] D. Bodea, A. Orbán, D. Ristoiu, and L. Nagy, J. Phys. B **31**, L745 (1998).
[106] N. Elander and E. Yarevsky, Phys. Rev. A **57**, 3119 (1998).
[107] M. Inokuti, Rev. Mod. Phys. **43**, 297 (1971); B. G. Tian and J. M. Li, Acta Phys. Sin. **33**, 1401 (1984).
[108] P. G. Burke, A. Hibbert, and W. D. Robb, J. Phys. B **4**, 153 (1971); K. A. Berrington, P. G. Burke, J. J. Chang, A. T. Chivers, W. D. Robb, and K. T. Taylor, Comput. Phys. Commun. **8**, 149 (1974); K. A. Berrington, P. G. Burke, M. Le Dourneuf, W. D. Robb, K. T. Taylor, and Lan Vo Ky, *ibid.* **14**, 346 (1978); K. A. Berrington, P. G. Burke, K. Butler, M. J. Seaton, P. J. Storey, K. T. Taylor, and Y. Yu, J. Phys. B **20**, 6379 (1987).
[109] K. A. Berrington, W. B. Eissner, and P. H. Norrington, Comput. Phys. Commun. **92**, 290 (1995), and references therein.
[110] L. Voky, H. E. Saraph, W. Eissner, Z. W. Liu, and H. P. Kelly, Phys. Rev. A **46**, 3945 (1992).
[111] J. M. Li, L. Voky, Y. Z. Qu, J. Yan, P.-H. Zhang, H. L. Zhou, and P. Faucher, Phys. Rev. A **55**, 3239 (1997).
[112] J. M. Li, L. Voky, J. Yan, and Y. Z. Qu, Chin. Phys. Lett. **13**, 902 (1996).
[113] X. Y. Han, L. Voky, and J. M. Li, Chin. Phys. Lett. **21**, 54 (2004).
[114] R. D. Cowan, *The Theory of Atomic Structure and Spectra* (University of California Press, Berkeley, 1981).
[115] NIST Atomic Spectra Database Levels Form, http://physics.nist.gov/cgi-bin/AtData/levels_form
[116] X. J. Liu, Y. P. Huang, L. F. Zhu, Z. S. Yuan, W. B. Li, and K. Z. Xu, Nucl. Instrum. Methods Phys. Res. A **508**, 448 (2003).